Ecosystems (2000) 3: 419–432
DOI: 10.1007/s100210000038

ECOSYSTEMS

ORIGINAL ARTICLES

Modeled Effects of Dissolved Organic Carbon and Solar Spectra on Photobleaching in Lake Ecosystems

Isabel Reche,* Michael L. Pace, and Jonathan J. Cole

Institute of Ecosystem Studies, Box AB, Millbrook, New York 12545-0129, USA

ABSTRACT

Dissolved organic matter (DOM) contains molecules that absorb light at various wavelengths. This chromophoric DOM (CDOM) influences the transmission of both visible and ultraviolet energy through water. The absorption of light by CDOM often causes structural changes that reduce its capacity to further absorb light, a process termed 'photobleaching'. A model was designed to assess photobleaching through the entire water column of lake ecosystems. The model uses lake morphometry and dissolved organic carbon (DOC) concentration in conjunction with a defined solar spectrum and experimentally measured photobleaching rates to compute the total water column photobleaching. The model was initially applied to a theoretical 'average' lake using solar spectra for both the north (N) and south (S) temperate western hemispheres and variable DOC from 0.3 to 30 mg L^{-1}. The consequences of varying waveband-specific photobleaching coefficients and lake morphometry were explored in a second set of simulations. Finally, the model was also applied to four temperate northern lakes for which we had prior measurements of CDOM photobleaching rates. The model demonstrates that all three wavebands of solar radiation (UVB, UVA, and PAR) contribute significantly to total water column photobleaching, with UVA being most important. The relative contributions of the three wavebands were invariant for DOC more than 3 mg L^{-1}. Total water column photobleaching at 440 nm was three to five times faster under the UV-enriched solar spectrum of the southern hemisphere. Increasing the lake's mean depth (from 0.37 to 9.39 m) resulted in five- or 15-fold slower rates of total water column photobleaching for DOC concentrations of 1 or 10 mg L^{-1}, respectively. Varying the waveband-specific photobleaching coefficients by 10-fold resulted in a similar change in total water column photobleaching rates. Applying the model to four specific lakes revealed that photobleaching for the entire water column would reduce CDOM light absorption by 50% in 18–44 days under summer conditions.

Key words: CDOM photobleaching; solar wavebands; ultraviolet radiation; lake ecosystems; dissolved organic carbon.

INTRODUCTION

Chromophoric dissolved organic matter (CDOM) is one of the most important sunlight-absorbing components in lakes (Scully and Lean 1994; Morris and others 1995). At high CDOM concentrations, lakes appear brown or 'stained' in color; whereas at low concentrations, they appear clear blue. Thus, the concentration and optical properties of CDOM strongly influence the appearance of lakes, and CDOM is associated with distinct differences in ecosystem conditions (Williamson and others 1999).

Received 17 November 1998; accepted 27 June 2000.
*Corresponding author's present address: Departmento de Biología Animal y Ecología, Facultad de Ciencias, Universidad de Granada, 18071 Granada, Spain; *e-mail:* ireche@ugr.es

CDOM loses absorptivity directly by sunlight exposure and indirectly through light-produced oxidants. Both the light energy absorbed directly by CDOM, as well as photogenerated oxidants, cause structural changes in CDOM that reduce its capacity to further absorb light, a process termed 'photobleaching' (Whipple 1914; Strome and Miller 1978; Kieber and others 1990; Backlund 1992). The loss of the ability to absorb sunlight by CDOM is linked to a breakdown of chromophoric sites and a reduction in molecular weight (Strome and Miller 1978; Allard and others 1994; Bertilsson and Allard 1996). Photochemical changes in CDOM alter the chemical composition (Kieber and others 1990; Wetzel and others 1995; Corin and others 1996) and increase the bioavailability of DOC (Geller 1986; Wetzel and others 1995; Lindell and others 1995; Reche and others 1998). Therefore, the changes promoted by CDOM photobleaching can affect lake metabolism by changing both energy transmission in the water column (Morris and Hargreaves 1997; Reche and others 1999) and bacterial carbon uptake and growth efficiency (Kieber and others 1989; Mopper and others 1991; Reche and others 1998).

CDOM photobleaching caused by ultraviolet-B (UVB, 280–320 nm), ultraviolet-A (UVA, 320–400 nm), or photosynthetically active radiation (PAR, 400–700 nm) depends on quantum yields and the incident total energy within each waveband. Maximum quantum yields for many photochemical processes are in the UVB range (Kieber and others 1990; Moran and Zepp 1997). However, total energy in this band is at least 10-fold less than in the visible band (Kirk 1994). The energy distribution among wavebands varies geographically, depending on the transmission of each radiation band through the atmosphere. Latitude, total air column ozone concentration, cloudiness, and tropospheric pollutants (Frederick and others 1989; Madronich and others 1995) modify the relative contribution, mostly of UVB and UVA, to total energy. In addition to the selective transmission of different wavebands through the atmosphere, the attenuation of solar radiation in water is also wavelength-dependent, and it is strongly related to dissolved organic carbon (DOC) concentration (Morris and others 1995) and its optical properties (Morris and Hargreaves 1997). Longer wavelengths penetrate deeper into the water column, whereas shorter wavelengths in the UVB and UVA range attenuate rapidly.

Therefore, the total photobleaching in the water column of lake ecosystems is a function of several factors including: (a) energy distribution among wavebands at the Earth's surface, (b) the attenuation of each waveband in the water column, (c) the specific photobleaching rates associated with each waveband, and (d) lake morphometry, which affects the volume of water susceptible to photobleaching. The relative importance of these factors for the process of CDOM photobleaching needs to be considered to assess the potential effects of lake-specific properties and environmental conditions. These interactions are of increasing interest because of the recognition that (a) DOC influences many ecological and biogeochemical processes in lakes, and (b) DOC is susceptible to change from stratospheric ozone reduction, acidification, eutrophication, climatic warming, and land use (Schindler and others 1992, 1996; Yan and others 1996).

CDOM photobleaching is measured as the loss of absorptivity over time for a given wavelength (Kieber and others 1990; Molot and Dillon 1997; Morris and Hargreaves 1997; Reche and others 1999). The ecological implications of CDOM photobleaching differ depending on the wavelength selected. For example, photobleaching measured at 440 nm has significant implications for photosynthetic potential (one of the chlorophyll-a absorption peaks is at 430 nm) relative to photobleaching measured at 320 nm. Photobleaching at the longer wavelength (440 nm) would increase the transmission of PAR through the water column, whereas photobleaching at the shorter wavelength would increase the transmission of potentially damaging UV radiation.

In the present work, a model was designed to assess how changes in both solar spectrum and DOC concentration would modify total water column photobleaching. We initially assumed constant lake morphometry and waveband-specific photobleaching coefficients for UVB, UVA, and PAR. We subsequently assessed how variability in specific photobleaching coefficients (for the three wavebands) and lake morphometry would modify total water column photobleaching. We also applied the model to four lakes to calculate how actual differences among systems in DOC, experimental photobleaching rates, and morphometry affect estimated water column photobleaching.

Methods

Experiment to Calculate Waveband-specific Photobleaching Coefficients

To determine the specific rates of CDOM photobleaching caused by UVB, UVA, and PAR, we performed an experiment using water from a stained lake (Old Man McMullen Pond, Norfolk, Connecticut, 41°57'N, 73°15'W). The experiment consisted of four treatments that manipulated the quality of

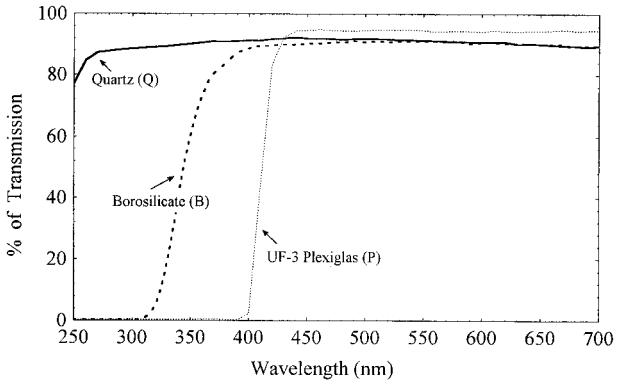

Figure 1. Percentage of energy transmission in the three experimental vessels (quartz, borosilicate, and UF-3 Plexiglas) as a function of wavelength measured on a spectrophotometer.

light exposure. For these treatments, water was incubated in either (a) quartz (Q) bottles, which permitted transmission of the entire solar spectrum (UVB + UVA + PAR); (b) borosilicate (B) bottles, which permitted transmission of most UVA and all PAR; (c) borosilicate bottles screened with UF-3 Plexiglas (P), which permitted transmission of PAR; or (d) dark bottles that allowed no light transmission (Figure 1).

All treatments were run in triplicate. Lake water was filtered through 0.22-μm Millipore filters to exclude particles and minimize bacterial influence. The bottles were exposed directly to natural sunlight for 2 days (from sunrise to sunset) at the Institute of Ecosystem Studies (IES; 41°50′N, 73°45′W). For absorbance measurements, subsamples were taken from each bottle seven to 10 times during the incubation period. The quartz and borosilicate bottles had inner diameters of 42 and 46 mm, respectively, and corresponding volumes of 200 and 300 ml. Although these bottles are not optically thin systems, their effects on measured photobleaching rates are small relative to the variation we consider in the model and the variation observed in photobleaching rates among systems (see Reche and others 1999).

CDOM absorbance was measured at 440 and 320 nm in a Shimadzu UV-visible recording spectrophotometer using 10-cm quartz cuvettes and expressed as absorptivity in m^{-1} (Miller 1998). Sunlight doses for the PAR waveband were measured at the IES site using a quantum sensor (LiCor model LI-190 SB). Sunlight doses for UVB and UVA were determined with a Biospherical Instruments Inc. (BSI) GUV-521 atmospheric sensor located at Lake Lacawac (41°23′N, 75°18′W) in northeastern Pennsylvania. IES and Lake Lacawac had similar atmospheric ozone concentration and air pollution during the incubation period of the experiment (based on a comparison of satellite ozone readings taken at the sites on the same dates). Therefore, we applied the Lake Lacawac PAR:UVA and PAR:UVB ratios to the IES site.

To obtain experimental photobleaching rates, we followed the procedures of Reche and others (1999). Because no significant changes in absorptivity were detected in the dark treatment, we attributed the loss of CDOM absorptivity to sunlight. Absorptivities decreased with increasing sunlight exposure, fitting negative exponential functions in transparent (Q, B, and P) treatments as:

$$a_{n\lambda Q,B,P} = a_{0\lambda}\, e^{-k_{b\lambda Q,B,P} D_{nQ,B,P}} \tag{1}$$

where $a_{n\lambda Q,\,B,\,P}$ are the absorptivities at λ = 440 or 320 nm after their corresponding sunlight doses (D_n). $D_{nQ,B,P}$ are the cumulative sunlight doses (Em^{-2}) for Q, B, and P treatments, respectively. The initial absorptivity is $a_{0\lambda}(m^{-1})$ at λ = 440 or 320 nm. Therefore, experimental photobleaching rates for each treatment ($k_{b\lambda Q,B,P}$) are the slopes of ln-absorptivities vs sunlight dose regressions:

$$\ln a_{n\lambda Q,B,P} = \ln a_{0\lambda} - k_{b\lambda Q,B,P} D_{nQ,B,P} \tag{2}$$

Waveband-specific photobleaching coefficients were then calculated from the subtraction of the regression slopes between treatments (*Q–B* and *B–P*), assuming no interactions among wavebands (see Discussion), as:

$$-k_{bUVB} = \frac{\ln a_{nQ} - \ln a_{nB}}{D_{nUVB}}$$

$$-k_{bUVA} = \frac{\ln a_{nB} - \ln a_{nP}}{D_{nUVA}}$$

$$-k_{bPAR} = \frac{\ln a_{0P} - \ln a_{nP}}{D_{nPAR}} \tag{3}$$

where k_{bUVB}, k_{bUVA}, and k_{bPAR} are the waveband-specific photobleaching coefficients associated with UVB, UVA, and PAR wavebands, respectively. D_{nUVB}, D_{nUVA}, and D_{nPAR} are the sunlight doses corresponding to UVB, UVA, and PAR bands. The ln-transformed absorptivities in Q, B, and P treatments after receiving sunlight doses are $\ln a_{nQ}$, $\ln a_{nB}$, and $\ln a_{nP}$.

Model for Lake Ecosystems

A model was designed to assess how changes in energy distribution among wavebands and DOC concentration could affect the loss of CDOM ab-

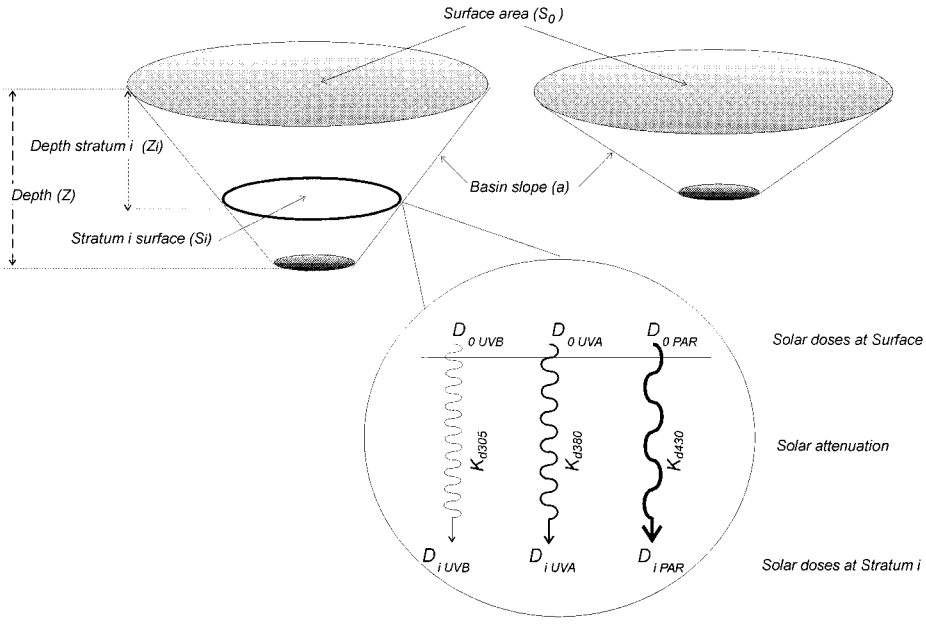

Figure 2. Schemes of lake morphometry for the model. Note that lake dimensions are not to scale. In the second set of simulations, we held constant S_o and bottom surface, varying the basin slopes (a) to obtain a range from steep-sided to shallow lakes. We also show details of nomenclature used to calculate the corresponding doses of UVB, UVA, and PAR that reach stratum i. See Table 1 for definitions.

sorptivity for an entire lake. We call this loss 'total water column photobleaching.' It is important to distinguish between this estimated result from the model and the waveband-specific photobleaching coefficients obtained from the experimental photobleaching rates (as measured in the experiment described above). DOC concentration and energy distribution among wavebands of the solar spectrum were used as variables in the model. Waveband-specific photobleaching coefficients (k_{bUVB}, k_{bUVA}, k_{bPAR}) were initially held constant, using values derived from the experiment. We varied these coefficients in subsequent simulations.

The model lake had a truncated conical shape, a maximum depth of 10 m, a surface area of 1 km^2, and a bottom area of 15,000 m^2. Morphometric parameters for the model lake were selected based on the high frequency of these attributes among world lakes (Wetzel 1990). This prototype lake was divided into 1000 vertical strata for the model calculations (Figure 2). The volume of each stratum (from i to j depths) was obtained using the equation:

$$V = \pi \int_i^j (b - az)^2 dz \qquad (4)$$

where b is surface radius, a is basin slope, and z is depth. Symbols and units for the model are summarized in Table 1.

The loss of CDOM absorptivity in each depth stratum is a function of the energy (sunlight doses) that reaches that stratum. Energy attenuation within the water column depends on wavelength (Kirk 1994) as well as the concentration and optical properties of DOC (Morris and others 1995). Sunlight doses for UVB, UVA, and PAR that reach each stratum were calculated according to the expressions:

$$D_{i\,UVB} = D_{oUVB}\, e^{-k_{d\,305} Z_i}\, S_i / S_0$$

$$D_{i\,UVA} = D_{oUVA}\, e^{-k_{d\,380} Z_i}\, S_i / S_0$$

$$D_{i\,PAR} = D_{oPAR}\, e^{-k_{d\,430} Z_i}\, S_i / S_0 \qquad (5)$$

where D_{iUVB}, D_{iUVA}, and D_{iPAR} are UVB, UVA, and PAR doses in stratum i (Em^{-2}); D_{oUVB}, D_{oUVA}, and D_{oPAR} are UVB, UVA, and PAR doses that reach the Earth's surface; $k_{d\,305}$, $k_{d\,380}$, and $k_{d\,430}$ (m^{-1}) are the diffuse attenuation coefficients for UVB, UVA, and PAR, respectively; S_i is area (m^2) of stratum i; S_0 is surface area (m^2); and Z_i is depth (m) of stratum i.

To assess the different effects of solar energy on photobleaching, two contrasting distributions of energy among wavebands were considered: (a) a historical minimum of stratospheric ozone concentration (Booth and others 1994) recorded in the southern hemisphere at Ushuaia, Argentina (54°35'S, 68°11'W), and (b) a typical summer condition for the northeastern United States at Millbrook, New York (41°50'N, 73°45'W). Diffuse attenuation coefficients were obtained from the empirical functions of Morris and others (1995). A wavelength of 430 nm was selected as representative of PAR attenuation because this wavelength is coincident with one of the chlorophyll-a absorbance peaks (Reynolds 1984) and only the shorter wavelengths within the PAR band have

Table 1. List of Symbols for Experiment and Model Equations

	Symbols	Definitions (units)
Experiment	$a_{n\lambda Q,B,P}$	Absorptivities after sunlight exposure in *Q*, *B*, and *P* treatments (m^{-1})
	$a_{0\lambda}$	Initial absorptivity (m^{-1})
	$k_{b\lambda Q,B,P}$	Experimental photobleaching rates in *Q*, *B*, and *P* treatments (($E\ m^{-2})^{-1}$)
	$D_{n\ Q,B,P}$	Sunlight doses received in the Q, B, and P treatments ($E\ m^{-2}$)
	$k_{b\lambda UVB,\ UVA,\ PAR}$	Waveband-specific photobleaching coefficients associated with *UVB*, with *UVA*, and with *PAR* (($E\ m^{-2})^{-1}$)
	$D_{n\ UVB,\ UVA,\ PAR}$	Solar doses corresponding to the *UVB, UVA, PAR* bands during incubation ($E\ m^{-2}$)
Model	$D_{i\ UVB,\ UVA,\ PAR}$	Solar doses corresponding to the *UVB, UVA, PAR* bands that reach stratum *i* ($E\ m^{-2}$)
	$D_{0\ UVB,\ UVA,\ PAR}$	Doses at surface level corresponding to *UVB, UVA, PAR* bands ($E\ m^{-2}$)
	$k_{d305},\ k_{d380},\ k_{d430}$	Diffuse attenuation coefficients representative for the *UVB, UVA, PAR* wavebands in water column (m^{-1})
	S_i	Area stratum *i* (m^2)
	S_0	Surface area (m^2)
	Z_i	Depth stratum *i* (m)
	$a_{i\lambda UVB,\ UVA,\ PAR}$	Absorptivities in the stratum *i* after the corresponding doses of D_{iUVB}, D_{iUVA}, and D_{iPAR} (m^{-1})
	$\bar{a}_{\lambda UVB,\ UVA,\ PAR}$	Water column mean absorptivities associated with UVB, UVA, and PAR (m^{-1}) weighted for the stratum volume (m^{-1})
	V_i	Volume stratum *i* (m^3)
	V_T	Total volume of lake (m^3)
	$-\Delta a_{\lambda UVBR,\ UVAR,\ PAR}$	Photobleaching due to UVB, UVA, and PAR (m^{-1})
	$-\Delta a_{\lambda TOTAL}$	Total photobleaching or loss of absorptivity in water column due to whole solar spectrum (m^{-1})
	$a_{\lambda TOTAL}$	Absorptivity in water column after total photobleaching (m^{-1})
	k_{wc}	Total water column photobleaching rate (d^{-1})
	$Half\text{-}life_\lambda$	Time to reduce 50% of the lake absorptivity at λ (d)

Absorptivity was measured at λ = 440 and 320 nm (m^{-1}).

been related to photobleaching (Morris and Hargreaves 1997).

The corresponding doses of each waveband that reach stratum $i(D_{i\ UVB}, D_{iUVA}, D_{i\ PAR})$ lead to losses of absorptivities following the general photobleaching model (Eq. 1):

$$a_{i\lambda UVB} = a_{0\lambda}\, e^{-k_{b\lambda UVB} D_{iUVB}}$$

$$a_{i\lambda UVA} = a_{0\lambda}\, e^{-k_{b\lambda UVA} D_{iUVA}}$$

$$a_{i\lambda PAR} = a_{0\lambda}\, e^{-k_{b\lambda PAR} D_{iPAR}} \quad (6)$$

where $a_{i\lambda\ UVB}$, $a_{i\lambda\ UVA}$, and $a_{i\lambda\ PAR}$ are the absorptivities at λ = 440 and 320 nm after receiving their corresponding doses; $k_{b\lambda\ UVB}$, $k_{b\lambda\ UVA}$, and $k_{b\lambda\ PAR}$ are experimental photobleaching rate coefficients caused by UVB, UVA, and PAR; and $a_{0\lambda}$ is the initial absorptivities at λ = 440 and 320 nm. These initial absorptivities were obtained from empirical regressions (y-intercept fixed at 0) between DOC concentration (mg l^{-1}) and absorptivities at 440 and 320 nm (m^{-1}) using data in Morris and others (1995). The functions were:

$$a_{0\ 440} = 0.324\ [DOC]\ (r^2 = 0.68,\ P < 0.001,\ n = 64)$$

$$a_{0\ 320} = 3.669\ [DOC]\ (r^2 = 0.67,\ P < 0.001,\ n = 64) \quad (7)$$

To obtain the mean absorptivities for an entire, well-mixed water column ($\bar{a}_{\lambda UVB}$, $\bar{a}_{\lambda UVA}$, $\bar{a}_{\lambda PAR}$), the absorptivities for each waveband and for each stratum *i* weighted for the stratum volume were integrated from surface level (0 m) to 10 m:

$$\bar{a}_{\lambda UVB} = \sum_{i=0}^{i=10} a_{\lambda iUVB} \frac{V_i}{V_T}$$

$$\bar{\mathbf{a}}_{\lambda UVA} = \sum_{i=0}^{i=10} a_{\lambda iUVA} \frac{V_i}{V_T}$$

$$\bar{\mathbf{a}}_{\lambda PAR} = \sum_{i=0}^{i=10} a_{\lambda iPAR} \frac{V_i}{V_T} \quad (8)$$

where V_i is volume of stratum i and V_T is lake volume.

The loss of absorptivity associated with each waveband ($-\Delta a_{\lambda UVB}$, $-\Delta a_{\lambda UVA}$, and $-\Delta a_{\lambda\ PAR}$), then, can be obtained as:

$$-\Delta a_{\lambda UVB} = a_{0\lambda} - \bar{\mathbf{a}}_{\lambda UVB}$$

$$-\Delta a_{\lambda UVA} = a_{0\lambda} - \bar{\mathbf{a}}_{\lambda UVA}$$

$$-\Delta a_{\lambda PAR} = a_{0\lambda} - \bar{\mathbf{a}}_{\lambda PAR} \quad (9)$$

Assuming no interactions among wavebands, total absorptivity loss ($-\Delta a_{\lambda\ TOTAL}$) is the sum of the absorptivity loss due to UVB ($-\Delta a_{\lambda\ UVB}$), UVA ($-\Delta a_{\lambda\ UVA}$), and PAR ($-\Delta a_{\lambda\ PAR}$). We refer to this as 'total water column photobleaching'—the quantity the model was designed to calculate.

We can express the total water column photobleaching ($a_{\lambda\ TOTAL} = a_{0\lambda} - \Delta a_{\lambda\ TOTAL}$) obtained for 1 day of solar exposure as a rate (k_{wc}):

$$-k_{wc} = \frac{\ln\left(\frac{a_{\lambda TOTAL}}{a_{0\lambda}}\right)}{t} \quad (10)$$

where t is time in days (solar doses expressed in d). It is convenient to express this rate as a half-life (the time to reduce 50% of the initial total CDOM absorptivity of the water column):

$$Half\text{-}life(d) = \frac{\ln(0.5)}{k_{wc}} \quad (11)$$

The relative contribution of each waveband to water column photobleaching was also calculated as:

$$Contribution\ UVB\ (\%) = \frac{-\Delta a_{\lambda UVB}}{-\Delta a_{\lambda TOTAL}} 100$$

$$Contribution\ UVA\ (\%) = \frac{-\Delta a_{\lambda UVA}}{-\Delta a_{\lambda TOTAL}} 100$$

$$Contribution\ PAR\ (\%) = \frac{-\Delta a_{\lambda PAR}}{-\Delta a_{\lambda TOTAL}} 100 \quad (12)$$

Simulations of the model (implemented in Statistica BASIC language) were performed with Statistica V5.1. The code for the model is available from I. R.

Simulations to Assess the Effects of Variation in Photobleaching Coefficients and Lake Morphometry on K_{wc}

In our initial analyses with the model, waveband-specific photobleaching coefficients and lake morphometry were held constant. In a second set of simulations, we varied these factors. Waveband-specific photobleaching coefficients were varied across an order of magnitude using the range of k_{bUVB} from 0.3 to 3 $(Em^{-2})^{-1}$ (in steps of 0.3) while maintaining the same original proportionality among the specific k_b values for UVB, UVA, and PAR as calculated from the experiment. The corresponding range of experimental photobleaching rates that involved the previous waveband-specific rates is similar to that measured among lakes by Reche and others (1999). To analyze the importance of lake morphometry, we varied the slope, a, in Eq. 4 from 500 to 20 while holding lake surface and bottom areas constant. At the extremes, the range of morphometries thus generated runs from steep-sided lakes with mean depths of 9.4 m to quite shallow lakes with mean depths of 0.4 m. DOC concentrations of 1 or 10 mg L^{-1} and the temperate northern hemisphere solar spectrum were used in these simulations.

Finally, we considered the implications of our model for a specific set of lakes for which we had previously measured photobleaching rates (Reche and others 1999). We estimated the total water column photobleaching for two soft-water lakes, Peter Lake and Paul Lake, located at the University of Notre Dame Environmental Research Center in northern Michigan and two hard-water lakes, Chodikee Lake and Stissing Lake, located in the Hudson Valley region of New York. The basic model was adjusted using measured experimental photobleaching rates, PAR attenuation coefficients, and morphometry for each lake.

Results

Experimental Determination of Specific Photobleaching Coefficients Associated with UVB, UVA, and PAR

CDOM absorptivities declined exponentially with sunlight dose, but rates varied by treatment (Figure 3). At both 440 nm and 320 nm, the highest losses in absorptivity were observed under the whole solar spectrum (Q treatment), whereas the lowest losses were seen under PAR (P treatment). Regressions between sunlight doses and the natural logs of the absorptivities had significant negative slopes in all cases, indicating that all wavebands contribute to

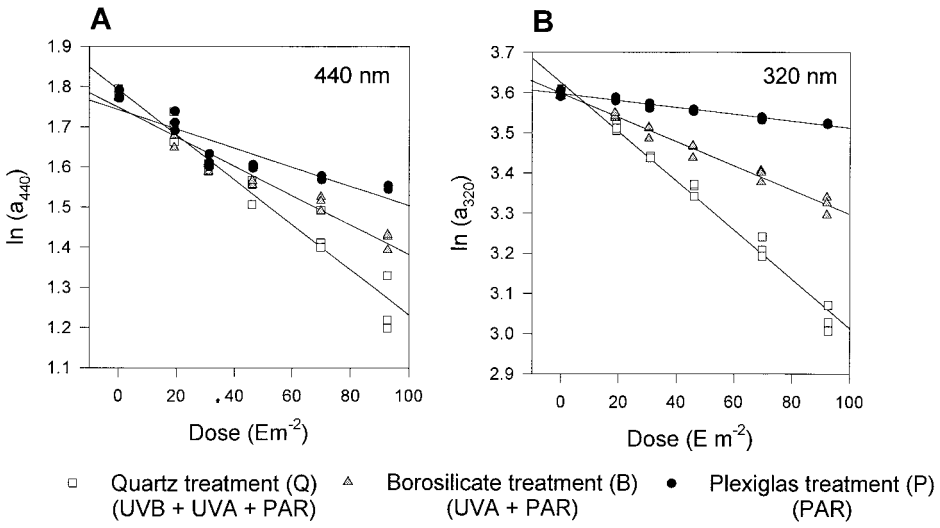

Figure 3. Changes in absorptivities at 440 nm (**A**) and at 320 nm (**B**) in the water of Old Man McMullen Pond under different cumulative sunlight doses in the treatments: quartz (UVB + UVA + PAR, white squares), borosilicate (UVA + PAR, gray triangles), and UF-3 Plexiglas (PAR, black circles). Note ln scale for absorptivities.

Table 2. Results of the Experiment Designed to Calculate Waveband-specific Photobleaching Coefficients using Water of Old Man McMullen Pond

		λ = 440 nm	λ = 320 nm
Experimental photobleaching rates	k_{bQ}	$56.09 \times 10^{-4} \pm 3.20 \times 10^{-4}$	$61.17 \times 10^{-4} \pm 1.83 \times 10^{-4}$
	k_{bB}	$36.65 \times 10^{-4} \pm 2.03 \times 10^{-4}$	$30.08 \times 10^{-4} \pm 1.04 \times 10^{-4}$
	k_{bP}	$24.52 \times 10^{-4} \pm 2.84 \times 10^{-4}$	$8.71 \times 10^{-4} \pm 0.44 \times 10^{-4}$
Waveband-specific photobleaching coefficients	k_{bUVB}	1.78 ± 0.41	2.85 ± 0.26
	k_{bUVA}	0.052 ± 0.013	0.088 ± 0.002
	k_{bPAR}	$24.52 \times 10^{-4} \pm 2.84 \times 10^{-4}$	$8.71 \times 10^{-4} \pm 0.44 \times 10^{-4}$

The photobleaching rates obtained at λ = 440 nm and λ = 320 nm in the different treatments: quartz (k_{bQ}), borosilicate (k_{bB}), and Plexiglas (k_{bP}) were used to calculate the waveband-specific photobleaching coefficients associated with UVB (k_{bUVB}), UVA (k_{bUVA}), and PAR (k_{bPAR}) (see Eq. 3).
K_b units = $(E\ m^{-2})^{-1}$

photobleaching. The rates of photobleaching (slopes) also differed depending on the wavelength used to measure absorbance. A higher slope was observed in the Q treatment for absorbances measured at 320 nm than for those measured at 440 nm. For the P treatment, the results were the reverse; a lower slope was observed for absorbances measured at 320 nm than for those measured at 440 nm (Table 2).

From the differences among treatments ($Q - B$ and B – P, Eq. 3), were calculated the photobleaching coefficients associated with UVB, UVA, and PAR (k_{bUVB}, kb_{UVA}, and k_{bPAR}) at both 440 nm and 320 nm (Table 2). The loss of absorptivity per UVB dose was two orders of magnitude higher than the loss of absorptivity per UVA dose, and the loss of absorptivity per UVA dose was one order of magnitude (at λ = 440 nm) or two orders of magnitude (at λ = 320 nm) higher than the loss of absorptivity per PAR dose. These photobleaching rates specific to each fraction of the solar spectrum (k_{bUVB}, k_{bUVA}, and k_{bPAR}) were used as constants in the initial model; we applied variations in these rates to a second set of simulations.

Lake Simulations

The variables for this model were DOC concentration (range, 0.3–30 mg L^{-1}) and solar spectrum quality. One spectrum represents a summer day at the IES site in the northern hemisphere (where the photobleaching measurements were made), with an energy distribution among UVB:UVA:PAR wavebands of 0.056:1.255:50 Em^{-2}. The other spectrum represents the extreme enrichment in the UVB and UVA wavebands seen at the southern hemisphere site of Ushuaia, Argentina, with a

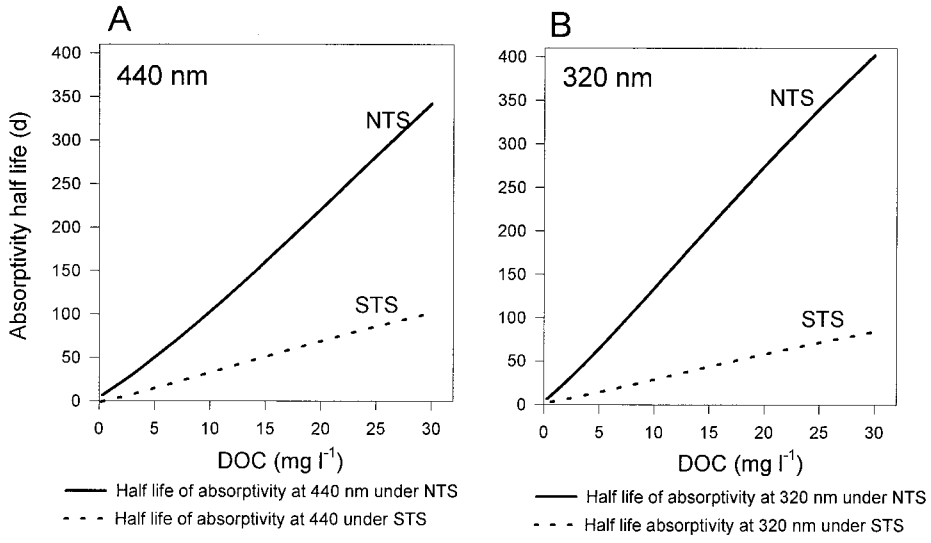

Figure 4. Simulation results for absorptivity half-lives at 440 nm (**A**) and 320 nm (**B**) under two solar spectra: northern temperate scenario (NTS, black lines) and southern temperate scenario (STS, dashed lines) and a wide range of DOC concentrations (from 0.3 to 30 mg L^{-1}).

UVB:UVA:PAR ratio of 0.624:9.276:50 Em^{-2}. UVB and UVA were respectively about 10- and sevenfold greater in the southern hemisphere spectrum. We refer to these two spectra as the NTS (northern temperate scenario) and the STS (southern temperate scenario). By comparing these scenarios, we can assess how the loss of absorptivity in lakes differs among regions in relation to UV exposure.

The result of photobleaching for a modeled lake is represented in terms of a half-life of absorptivity (that is, the time to reduce CDOM absorptivity by 50%). Thus, faster photobleaching means a shorter half-life (faster loss of absorptivity) as was the case for the STS compared with the NTS at all DOC concentrations (Figure 4). An increase in DOC concentration yields a longer half-life. For example, the half-life at 440 nm in the NTS was 6.6 d for a DOC concentration of 0.3 mg l^{-1} and 342 d for a DOC concentration of 30 mg l^{-1}. The half-life of absorptivity at 440 nm in the STS for an identical range of DOC concentrations varied from 1.2 d to 103 d. Therefore, under the scenario of UV-enriched conditions, the half-life of absorptivity at 440 nm was three- to fivefold faster in the STS depending on the DOC concentration. Half-life at 320 nm followed a similar pattern; it was five- to eightfold faster in the STS than in the NTS, depending on DOC (Figure 4B). The differences in absorptivity half-life in the STS compared with the NTS were more pronounced at 320 nm than at 440 nm.

One goal of the model was to assess the relative contribution of each waveband to total water column photobleaching. In the NTS, PAR was the waveband that contributed to the greatest loss of absorption at 440 nm (Figure 5A). This contribution ranged from 50% for lakes with a low DOC to about 70% for lakes with a high DOC. The UVB contribution to total water column photobleaching (at 440 nm) in the NTS decreased from 25% to around 10% as DOC increased. The UVA contribution was very stable (at about 25%) across the DOC range (Figure 5A). However, in the ultraviolet-enriched conditions of the STS, UVA accounted for about 50% of water column photobleaching and was the dominant waveband (Figure 6A). The UVB contribution decreased from about 50% to 30% as DOC increased. The PAR contribution followed the same pattern as the UVA one, but with lower values (from 10% to 20%) (Figure 6A). The most significant difference between the two scenarios was the PAR contribution to water column photobleaching at 440 nm, which was less than 20% for the STS and more than 50% for the NTS.

At 320 nm, UVA was the major waveband involved in total water column photobleaching (Figures 5B and 6B). The contribution of UVA increased only slightly with DOC in the NTS scenario (from around 45% to 50%), whereas the change was greater for the STS (around 45%–60%). PAR was generally more important than UVB to water column photobleaching in the NTS. Alternatively, UVB was significantly more important in the STS, contributing about 35%, whereas PAR accounted for less than 10%, irrespective of DOC concentration (Figure 6B). Asymptotes for the contributions of each waveband to total water column photobleaching were reached at relatively low DOC concentrations. These contributions were almost constant for lakes with DOC concentrations of more than 3 mg L^{-1} for both solar spectra.

To assess how waveband-specific photobleaching coefficients and lake morphometry influence total

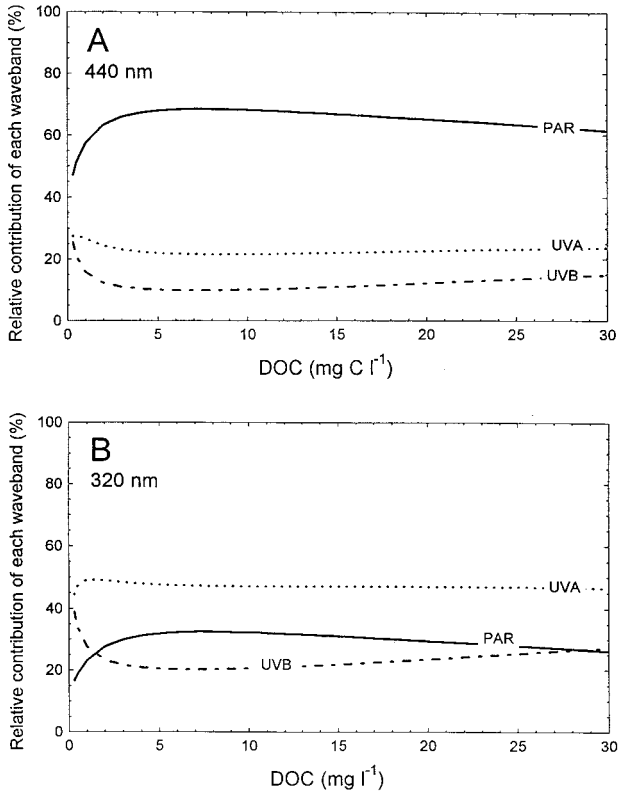

Figure 5. Simulation results for the relative contribution of UVB, UVA, and PAR to total water column photobleaching measured as loss of absorptivity at 440 nm (**A**) and 320 nm (**B**) under the solar spectrum of the IES site (NTS).

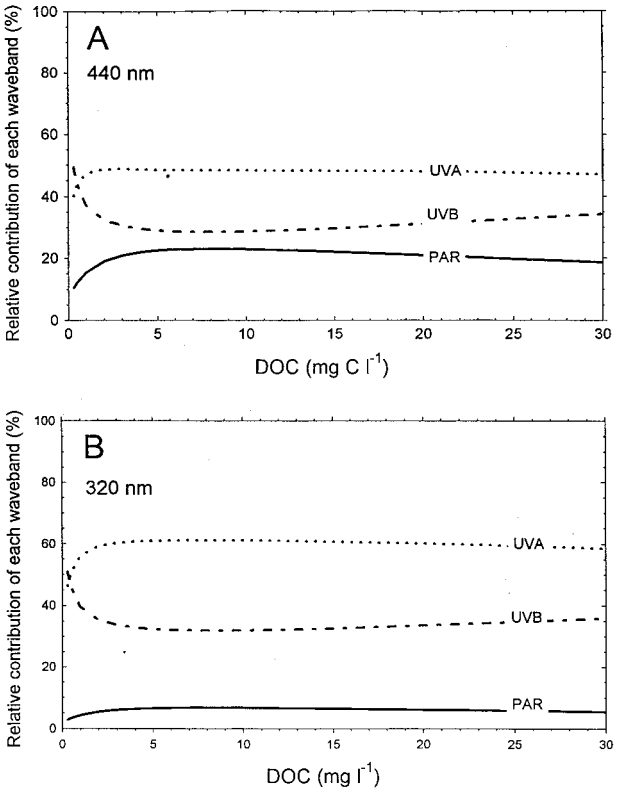

Figure 6. Simulation results for the relative contribution of UVB, UVA, and PAR to total water colum photobleaching measured as loss of absorptivity at 440 nm (*A*) and 320 nm (*B*) under the solar spectrum of the Ushuaia site (STS).

water column photobleaching was performed for another set of simulations (Figure 7). In this case, the DOC concentration (1 or 10 mg L^{-1}) and its optical properties (a_{440}:DOC ratio = 0.2) were fixed. To simplify the presentation of the results, the three waveband-specific photobleaching coefficients used in each simulation were represented by the corresponding values of the experimental photobleaching rate in quartz (k_{bQ}). This substitution also facilitates the comparison with previous studies in which experimental photobleaching rates were calculated (for example, Reche and others 1999). Variability in morphometry considered in this set of simulations (lake mean depths from 0.37 m to 9.39 m) resulted in changes in absorptivity half-life of about fivefold for a DOC concentration of 1 mg L^{-1} and about 15-fold for a DOC concentration of 10 mg L^{-1}, irrespective of the waveband-specific photobleaching coefficient selected. The effects of lake morphometry can be observed by comparing the half-life values for constant waveband-specific photobleaching coefficients in lakes with different mean depths. For example, for a k_{bQ} of 18.9×10^{-4} $(Em^{-2})^{-1}$ ($k_{bUVB} = 0.6$ $(Em^{-2})^{-1}$, $k_{bUVA} = 0.0175$ $(Em^{-2})^{-1}$, $k_{bPAR} = 8.3 \times 10^{-4} (Em^{-2})^{-1}$) and 1 mg l^{-1} of DOC, the modeled absorptivity half-life is 18.8 d for a lake with a mean depth of 0.94 m and 75.2 d for a lake with a mean depth of 9.39 m (Figure 7A, dashed lines).

The 10-fold variability in the waveband-specific photobleaching coefficients considered in this second set of simulations results in a 10-fold change in absorptivity half-life for any given mean depth. The effects of different waveband-specific photobleaching variabilities can be assessed by comparing half-lives for a constant mean depth. For a lake with a mean depth of 3.79 m, 10 mg l^{-1} of DOC, and a ratio of a_{440} to DOC of 0.2, the half-life is 297.2 d for a k_{bQ} of 18.9×10^{-4} $(Em^{-2})^{-1}$ and 68.0 d for a k_{bQ} of 85.1×10^{-4} $(Em^{-2})^{-1}$ (Figure 7B, dashed lines).

Photobleaching in Specific Lakes

Estimated values of water column absorptivity half-life at 440 nm varied from 18.1 to 44.2 d in the four lakes for which we had data on experimental pho-

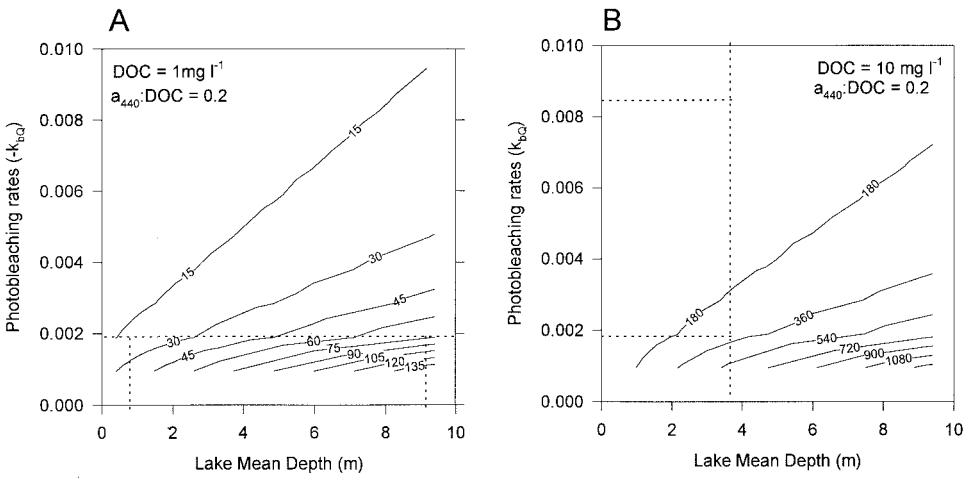

Figure 7. Simulation results for absorptivity half-lives at 440 nm for a constant DOC concentration of 1 mg l^{-1} (*A*) or 10 mg l^{-1} (*B*), a constant a_{440}: DOC ratio (0.2) and variable lake mean depths and waveband-specific photobleaching coefficients. On the y-axis, we show only the corresponding values of the experimental photobleaching rates in quartz (k_{bQ}) to simplify. Numbers on the isopletes are absorptivity half-lives in days.

Table 3. Results of the Model Simulations for Four Specific Lakes, Morphometries and DOC Properties

Lakes	Location	a_{440} (m^{-1})	DOC (mg l^{-1})	k_{dPAR} (m^{-1})	Mean Depth (m)	$k_b \times 10^{-4}$ (E $m^{-2})^{-1}$	Absorptivity[c] Half-life (d)
Paul	46°13′N, 89°32′W	1.4	4.0	0.77	3.7	7.0 ± 1.9[a]	26.3
Peter	46°13′N, 89°32′W	2.2	7.7	0.99	5.7	22.9 ± 1.1[a]	44.2
Chodikee	41°46′N, 74°9′W	3.7	7.7	2.10	2.8	45.4 ± 3.8[b]	22.2
Stissing	41°50′N, 73°37′W	1.1	4.2	1.16	4.6	51.8 ± 8.1[b]	18.1

[a, b] *Experimental photobleaching rates in borosilicate (k_{bB}) or quartz bottles (k_{bQ}) ± standard errors obtained by Reche and others (1999)*
Paul and Peter lakes are located in the University of Notre Dame Environmental Research Center (MI); Chodikee and Stissing lakes are located in the Hudson Valley (NY).
[c] At 440 nm.

tobleaching rates, morphometry, and a_{440}: DOC (Table 3). The lake with maximum mean depth (5.7 m), Peter Lake, had the longest half-life, whereas the lake with the fastest experimental photobleaching rate, Stissing Lake, had the shortest half-life. Peter and Chodikee lakes had equivalent DOC concentrations (7.7 mg l^{-1}) but different mean depths (5.7 and 2.8 m, respectively) and experimental photobleaching rates ($k_{bB} = 22.9 \times 10^{-4}$ and $k_{bQ} = 45.4 \times 10^{-4}$, respectively). Half-lives differed by a factor of two, reflecting the combined effects of morphometry and experimental photobleaching rates. Table 3 also suggests that in lakes with relatively similar a_{440}:DOC ratios and mean depths, such as Peter and Stissing lakes, the differences observed in absorptivity half-life are driven by the experimental photobleaching rates (derived from measurements in these lakes; see Methods). These differences in experimental photobleaching rates are closely related to lake chemical conditions and strongly correlated with alkalinity (Reche and others 1999). Thus, Stissing, a high-alkalinity lake, has faster photobleaching and a shorter absorptivity half-life than Peter, a low-alkalinity lake.

DISCUSSION

Model Results

Most photobleaching studies are only applicable to the uppermost sunlit depths of natural waters. Although models have been proposed for other photochemical processes (Scully and others 1997), the model proposed in this work is the first attempt to estimate photobleaching at the scale of an entire lake. A major finding of the current study is that UVA and PAR, not just UVB, play an important role in photobleaching when it is estimated for the entire water column. The model also demonstrates that all wavebands of the solar spectrum contribute to total water column photobleaching (Figures 5 and 6). Two important features of the model are accounting for the loss of light energy with increasing depth and the variable exposure of depth strata depending

on lake morphometry. These factors are critical in determining photobleaching at an ecosystem scale.

It is well established that quantum-yield spectra of specific photochemical reactions are generally greater in the UVB range and tail to zero in the UVA or PAR range (Kieber and others 1990; Scully and others 1996; Moran and Zepp 1997; Miller 1998). CDOM complexity, however, prevents a precise definition of the molar concentration of chromophores present and restricts the use of quantum yield for CDOM photobleaching (Miller 1998). Nevertheless, waveband-specific photobleaching coefficients caused by UVB were higher than specific photobleaching coefficients associated with UVA or PAR (compare k_{bUVB}, k_{bUVA}, k_{bPAR} in Table 2). However, the model reveals that because of the rapid attenuation of UVB with depth in the water column, UVA and PAR often account for a large fraction of water column photobleaching.

The model also illustrates how water column photobleaching differs depending on the wavelength at which this process is measured (for example, 440 nm compared to 320 nm). Thus, in a study focused, for example, on primary producers, photobleaching measured at wavelengths close to chlorophyll-a absorption peaks (that is, 440 nm) is relevant for understanding changes in photosynthetic potential. In fact, DOC concentrations have been reported as important controlling factors of primary production (Jones 1992; Carpenter and others 1998); thus, photobleaching may interact with photosynthesis by affecting light availability.

Application of the model to specific lakes reveals that the photobleaching process can be extremely rapid, with half the absorptivity lost in 18–44 days (Table 3). Thus, with no new input or formation of CDOM, we would expect the four lakes we studied to 'clear' over the course of a summer. We have weekly data on absorbance for Paul and Peter lakes over several summers, and such a clearing as a result of photobleaching does not occur. The values of a_{440} are relatively constant (data not shown). This means that photobleaching is balanced by new inputs or other, as yet poorly understood processes that generate CDOM in lakes.

Model Limitations

The model was designed to assess how different solar spectra and differences in DOC concentration (via energy attenuation in the water column) modify the loss of CDOM absorptivity for a water column. In designing this model, we made several simplifying assumptions. Initially, we considered a specific lake morphometry and fixed waveband-specific photobleaching coefficients, but we varied these factors in subsequent simulations to explore the consequence of these two assumptions. The variability in the waveband-specific photobleaching coefficients considered in the second set of simulations represents the experimental range obtained by Reche and others (1999). We also assumed a well-mixed water column to simplify the model; however, recent evidence suggests that mixing can significantly affect CDOM photobleaching (H. Zagarese personal communication).

We selected k_{d305}, k_{d380}, and k_{d430} as representative diffuse attenuation coefficients for the whole UVB, UVA, and PAR bands, respectively. We used an intermediate wavelength for UVB and UVA bands to simplify the estimate of their corresponding attenuations. Integration of all wavelength-specific coefficients is expected to be close to the intermediate value we chose, but that depends on the nature of the function that describes the change in coefficients with wavelength. In the case of PAR attenuation, 430 nm was used because photobleaching is caused only by the shorter PAR wavelengths (Morris and Hargreaves 1997), and 430 nm is also a chlorophyll-a absorption peak. Diffuse attenuation coefficients were used to estimate the solar energy of each waveband that reaches the different strata, and we assumed that these coefficients were functions of DOC, as proposed by Morris and others (1995).

The use of the entire PAR waveband introduces some error into our estimates of PAR attenuation in the water column based on our use of an attenuation coefficient for 430 nm. Improvements to our model in the context of PAR would require more wavelength-specific measurements of (a) PAR at ground level, (b) PAR attenuation in the water column, and (c) photobleaching. The latter measurements (that is, wavelength-specific rates of photobleaching by PAR) are currently quite limited, consisting of measurements made at only a few wavelengths and using wide wavebands as solar doses.

To calculate the waveband specific photobleaching rate coefficients, no significant interaction among wavebands in photobleaching was assumed (Eq. 3). Different fractions of the solar spectrum can have opposing effects on other photobiological processes. For example, UVB causes DNA damage, reducing growth; but UVA and PAR can induce repair of that damage (Zagarese and others 1997). Such effects have not been described for photobleaching, so we cannot yet characterize them in a model.

Our model does not account for the effects of particles. Light-scattering by particulate matter and light absorption by phytoplankton can be important

factors in light transmission (Kirk 1983). Our model is only concerned with the interactions of dissolved matter and light. This assumption is reasonable for lakes where DOC is the major regulator of light, but it is less adequate for highly eutrophic and/or turbid lakes, where light attenuation by particles is significant (Kirk 1983).

Ideally, we would compare the results of our model to data on photobleaching. However, there are no direct measurements that we are aware of for water column photobleaching in lake ecosystems. Such measurements would require detailed depth profiles of photobleaching over time. Further, the process is difficult to estimate indirectly by balancing photobleaching against other processes, because there are few data on the rates of CDOM input and formation in lakes. Thus, at this point, our model is exploratory. It would require better measurements of photobleaching in lake ecosystems in order to be used as an analytical tool for the rigorous evaluation of hypotheses about photobleaching in the context of model prediction and data analysis.

Inferences from the Model

The model suggests how solar spectrum quality, DOC concentration, and DOC optical properties (photobleaching variability and a_{440}:DOC ratio) influence total water column photobleaching. These factors interact with environmental conditions that can induce both changes in solar spectrum quality (Madronich and others 1995) and changes in DOC concentrations or properties (De Haan 1992; Schindler and others 1992, 1996, 1997). Stratospheric ozone concentration plays a major role in controlling the amount of UVB that reaches ground level (McKenzie and others 1991; Madronich 1992), but tropospheric ozone, aerosols, and pollutants also affect the UVA and UVB that reaches the Earth's surface (Cabrera and others 1995). Therefore, natural factors (latitude, altitude, climatology, and so on) and anthropogenic factors (stratospheric ozone concentration, aerosols, gaseous pollutants, and so on) can modify solar spectrum quality (the UVB:UVA:PAR ratio). The model analysis indicates that solar spectrum quality has a clear impact on absorptivity half-life (Figure 4). A solar spectrum enriched in ultraviolet radiation (as in the STS, where ozone depletion is significant) causes rapid photobleaching. The consequent faster loss of absorptivity under those conditions will reduce UV attenuation, resulting in deeper penetration of this radiation through the water column.

The model demonstrates that when the entire water column is considered, both UVA and PAR have significant effects on photobleaching and that under some circumstances (that is, in high-DOC lakes in the north temperate zone) UVB may be of minor significance. The contributions of each waveband to total photobleaching were dependent on solar energy distribution among wavebands (NTS vs STS), wavelength selection used to measure absorptivity (440 nm vs 320 nm), and DOC concentration. The intermediate penetration (Morris and others 1995) and specific photobleaching coefficients associated with UVA result in this waveband making, in most cases, the greatest contribution to water column photobleaching, particularly in lakes with DOC concentrations greater than 3 mg L^{-1}. The only exception was for the NTS scenario in which the greatest contribution to water column photobleaching was by PAR at 440 nm (Figure 5A). Therefore, the effect of PAR on water column photobleaching is related to solar spectrum quality and the wavelength used to measure absorption. Potential increases in the UVB fraction of the solar spectrum due to stratospheric ozone depletion (McKenzie and others 1991; Madronich 1992) could lead to a reduction in the role of PAR in total water column photobleaching.

Based on the model simulations, absorptivity half-life is expected to lengthen as DOC concentration increases (Figure 4) and to shorten as measured photobleaching rates increase (Figure 7). Therefore, environmental conditions that modify DOC and its optical photoreactivity are critical processes in aquatic systems (Schindler and others 1996).

Watershed inputs are important in determining DOC concentrations in lakes (Rasmussen and others 1989; Caraco and Cole forthcoming). Chemical conditions within lakes are also important in determining DOC concentrations and photobleaching rates. For example, anthropogenic acidification can decrease the solubility of humic substances, inducing coagulation and sedimentation (De Haan and others 1983) and ultimately leading to a reduction in DOC. Reche and others (1999) found that alkalinity and ionic strength are strongly correlated to the variability in experimental photobleaching rates observed among lakes. High alkalinities are associated with accelerated photobleaching. Anthropogenic factors that promote in-lake alkalinity generation—for example, climatic warming (Psenner and Schmidt 1992; Schindler and others 1996; Sommaruga-Wögrath and others 1997)—may therefore indirectly increase photobleaching.

Eutrophication may also affect chromophoric DOC concentrations due to the enhanced utilization of this carbon source by bacteria under phos-

phorus-enriched conditions (Zweifel and others 1995; Reche and others 1998). Other environmental perturbations, such as forest fires and floods, may increase DOC inputs in lakes (Schindler and others 1992; Kelly and others 1997). Some of these environmental stresses have opposing effects on DOC concentration and light attenuation and consequently on photobleaching.

Complex physical, chemical, and biological processes influence the concentration, composition, and optical properties (for example, the chromophoric content) of DOC in aquatic ecosystems. Absorptivity is one of the most critical properties of DOC, because the penetration of PAR and UV influences many ecological interactions and processes. Our study shows that the photochemical dynamics that determine absorptivity may be dependent on ecosystem size and shape and absolute concentration of DOC, as well as light energy input across the wavebands of ultraviolet and short visible light. These effects interact to influence the concentration and optical qualities of DOC. Further work is still needed to integrate the processes leading to the input and production of DOC with factors such as light exposure and photobleaching, which cause both the loss and transformation of DOC. This work will help us to characterize the dynamics of DOC and understand the effects of changing environmental conditions (for example, climate, UV exposure) on the ecological interactions in aquatic ecosystems.

ACKNOWLEDGMENTS

We thank D. Thomas, D. Fisher, and V. Kelly for their assistance in the lab and with the radiation data. D. Morris and B. Hargreaves provided data on ultraviolet radiation and helpful discussion. F. Perfectti provided wise advice on model design and computing. We also thank R. Sommaruga, H. Zagarese, D. McKnight, and several anonymous reviewers for their valuable comments. This research was supported by a National Science Foundation grant to M.L.P. and J.J.C. and a postdoctoral fellowship from the Spanish Ministerio de Education y Ciencia MEC to I.R.

REFERENCES

Allard B, Borén H, Petterson C, Zhang G. 1994. Degradation of humic substances by UV-irradiation. Environ Int 20:97–101.

Backlund P. 1992. Degradation of aquatic humic material by ultraviolet light. Chemosphere 25(12):1869–78.

Bertilsson S, Allard B. 1996. Sequential photochemical and microbial degradation of refractory dissolved organic matter in a humic freshwater system. Arch Hydrobiol Spec Issues Adv Limnol 48:133–41.

Booth CR, Lucas TB, Morrow JH, Weiler CS, Penhale PA. 1994. The United States National Science Foundation's polar network for monitoring ultraviolet radiation. Antarctic Res Ser 62:17–37.

Caraco, NF, Cole JJ. When terrestrial organic matter is sent down the river: importance of allochthonous C inputs to the metabolism in lakes and rivers. In: Polis GA, Power ME, editors. Food webs at the landscape level. Forthcoming.

Cabrera S, Bozzo S, Fuenzalida H. 1995. Variations in UV radiation in Chile. J Photochem Photobiol 28:137–42.

Carpenter SR, Cole JJ, Kitchell JF, Pace ML. 1998. Impact of dissolved organic carbon, phosphorus and grazing on phytoplankton biomass and production in experimental lakes. Limnol Oceanogr 43:73–80.

Corin N, Backlund P, Kulovaara M. 1996. Degradation products formed during UV-irradiation of waters. Chemosphere 33: 245–55.

De Haan H. 1992. Impacts of environmental changes on the biogeochemistry of aquatic humic substances. Hydrobiologia 229:59–71.

De Haan H, Werlemark G, De Boer T. 1983. Effect of pH on molecular weight and size of fulvic acid in drainage water from peaty grass-land in NW Netherlands. Plant Soil 75:63–73.

Frederick JE, Snell HE, Haywood EK. 1989. Solar ultraviolet radiation at the Earth's surface. Photochem Photobiol 50(8): 443–50.

Geller A. 1986. Comparison of mechanisms enhancing biodegradability of refractory lake water constituents. Limnol Oceanogr 31:775–64.

Jones RI. 1992. The influence of humic substances on lacustrine planktonic food chains. Hydrobiologia 229:73–91.

Kelly CA, Rudd JWM, Bodaly RA, Roulet NP, St. Louis VL, Heyes A, Moore TR, Schiff S, Aravena R, Scott KJ, Dyck B, Harris R, Warner B, Edwards G. 1997. Increases in fluxes of greenhouse gases and methyl mercury following flooding of an experimental reservoir. Environ Sci Tech 31:1334–44.

Kieber DJ, McDaniel J, Mopper K. 1989. Photochemical source of biological substrates in sea water: implications for carbon cycling. Nature 341:637–69.

Kieber DJ, Zhou X, Mopper K. 1990. Formation of carbonyl compounds from UV-induced photodegradation of humic substances in natural waters: fate of riverine carbon in the sea. Limnol Oceanogr 35:1503–15.

Kirk JTO. 1983. Light and photosynthesis in aquatic ecosystems. Cambridge University Press: New York, 401 p.

Kirk JTO. 1994. Optics of UV-B radiation in natural waters. Arch Hydrobiol Beih Ergebn Limnol 43:1–16.

Lindell MJ, Granéli W, Tranvik LJ. 1995. Enhanced bacterial growth in response to photochemical transformation of dissolved organic matter. Limnol Oceanogr 40:195–9.

Madronich S. 1992. Implications of recent total atmospheric ozone measurements for biologically active ultraviolet radiation reaching the Earth's surface. Goephys Res Lett 19:37–40.

Madronich S, McKenzie RL, Caldwell MM, Björn LO. 1995. Changes in ultraviolet radiation reaching the Earth's surface. Ambio 24(3):143–52.

McKenzie RL, Matthews WA, Johnston PV. 1991. The relationship between erythemal UV and ozone, derived from spectral irradiance measurements. Geophys Res Lett 18:2269–72

Miller WL. 1998. Effects of UV radiation on aquatic humus: photochemical principles and experimental considerations. In: Hessen DO, Tranvik LJ, editors. Aquatic humic substances.

Ecological Studies, vol. 133. Berlin Heidelberg: Springer-Verlag p 125–45.

Molot LA, Dillon PJ. 1997. Photolytic regulation of dissolved organic carbon in northern lakes. Global Biogeochem Cy 11(3):357–65.

Mopper K, Zhou X, Kieber RJ, Kieber DJ, Sikorski RJ, Jones RD. 1991. Photochemical degradation of dissolved organic carbon and its impact on the oceanic carbon cycle. Nature 353:60–2.

Moran MA, Zepp RG. 1997. Role of photoreactions in the formation of biologically labile compounds from dissolved organic matter. Limnol Oceanogr 42:1307–16.

Morris DP, Hargreaves BR. 1997. The role of photochemical degradation of dissolved organic carbon in regulating the UV transparency of three lakes on the Pocono Plateau. Limnol Oceanogr 42:239–49.

Morris DP, Zagarese H, Williamson CE, Balseiro EG, Hargreaves BR, Modenutti B, Moeller R, Queimalinos C. 1995. The attenuation of solar UV radiation in lakes and the role of dissolved organic carbon. Limnol Oceanogr 40:1381–91.

Psenner R, Schmidt R. 1992. Climate-driven pH control of remote alpine lakes and effect of acid deposition. Nature 356: 781–3.

Rasmussen JB, Godbout L, Schallenberg M. 1989. The humic content of lake water and its relationship to watershed and lake morphometry. Limnol Oceanogr 34:1336–43.

Reche I, Pace ML, Cole JJ. 1998. Interactions of photobleaching and inorganic nutrients in determining bacterial growth on colored dissolved organic carbon. Microb Ecol 36:270–80.

Reche I, Pace ML, Cole JJ. 1999. Relationship of trophic and chemical conditions to photobleaching of dissolved organic matter in lake ecosystems. Biogeochemistry 44:259–80

Reynolds CS. 1984. The ecology of freshwater phytoplankton. Cambridge University Press 384 p

Schindler DW, Bayley SE, Curtis PJ, Parker BR, Stainton MP, Kelly CA. 1992. Natural and man-caused factors affecting the abundance and cycling of dissolved organic substances in Precambrian shield lakes. Hydrobiologia 229:1–21.

Schindler DW, Curtis PJ, Bayley SE, Parker BR, Beaty KG, Stainton MP. 1997. Climate-induced changes in the dissolved organic carbon budgets of boreal lakes. Biogeochemistry 36:9–28.

Schindler DW, Curtis PJ, Parker BR, Stainton MP. 1996. Consequences of climate warming and lake acidification for UV-B penetration in North American boreal lakes. Nature 379:705–708.

Scully NM, Lean DRS. 1994. The attenuation of ultraviolet light in temperate lakes. Ergeb Limnol 43:135–44.

Scully NM, McQueen DJ, Lean DRS, Cooper WJ. 1996. Hydrogen peroxide formation: the interaction of ultraviolet radiation and dissolved organic carbon in lake waters along a 43–75° N gradient. Limnol Oceanogr 41:540–48.

Scully NM, Vincent WF, Lean DRS, Cooper WJ. 1997. Implications of ozone depletion for surface-water photochemistry: sensitivity of clear lakes. Aquat Sci 59:260–74.

Sommaruga-Wögrath S, Koining KA, Schmidt R, Sommaruga R, Tessadri R, Psenner R. 1997. Temperature effects on the acidity of remote alpine lakes. Nature 387:64–7.

Strome DJ, Miller MC. 1978. Photolytic changes in dissolved humic substances. Verh Int. Verein Limnol 20:1248–54.

Wetzel RG. 1990. Land-water interfaces: metabolic and limnological regulators. Verh Int. Verein Limnol 24:6–24.

Wetzel RG, Hatcher PG, Bianchi TS. 1995. Natural photolysis by ultraviolet irradiance of the recalcitrant dissolved organic matter to simple substrates for rapid bacterial metabolism. Limnol Oceanogr 40:1369–80.

Whipple GC. 1899. The microscopy of drinking water. Wiley: New York, 300 p.

Williamson CE, Morris DP, Pace ML, Olson OG. 1999. Dissolved organic carbon and nutrients as regulators of lake ecosystems: resurrection of a more integrated paradigm. Limnol Oceanogr 44:795–803.

Yan ND, Keller W, Scully NM, Lean DRS, Dillon PJ. 1996. Increased UV-B penetration in a lake owing to drought-induced acidification. Nature 381:141–3.

Zagarese HE, Feldman M, Williamson CE. 1997. UV-B induced damage and photoreactivation in three species of *Boeckella* (Copepoda, Calanoida). J Plankton Res 19:357–67.

Zweifel UL, Wikner J, Hagstrom A, Lundberg E, Norrman B. 1995. Dynamics of dissolved organic carbon in a coastal ecosystem. Limnol Oceanogr 40:299–305.